In-Situ Spectroscopy of Water Oxidation at Ir Oxide Nanocluster Driven by Visible TiOCr Charge-Transfer Chromophore in Mesoporous Silica

Hongxian Han and Heinz Frei*

Physical Biosciences Division, Lawrence Berkeley National Laboratory,

University of California, Berkeley, CA 94720

(*J. Phys. Chem. C*, submitted)

Abstract

An all-inorganic photocatalytic unit consisting of a binuclear TiOCr charge-transfer chromophore coupled to an Ir oxide nanocluster has been assembled on the pore surface of mesoporous silica AlMCM-41. In situ FT-Raman and EPR spectroscopy of an aqueous suspension of the resulting Ir_xO_y-TiCr-AlMCM-41 powder reveal the formation of superoxide species when exciting the Ti(IV)OCr(III) → Ti(III)OCr(IV) metal-to-metal charge-transfer chromophore with visible light. Use of $H_2{}^{18}O$ confirms that the superoxide species originates from oxidation of water. Photolysis in the absence of persulfate acceptor leads to accumulation of Ti(III) instead. The results are explained by photocatalytic oxidation of water at Ir oxide nanoclusters followed by trapping of the evolving O_2 by transient Ti^{III} centers to yield superoxide. Given the flexibility to select donor metals with appropriate redox potential, photocatalytic units consisting of a binuclear charge-transfer chromophore coupled to a water oxidation catalyst shown here constitute a step towards thermodynamically efficient visible light water oxidation units.

1. Introduction

Inorganic molecular or well-defined polynuclear photocatalytic units on inert nanoporous oxide supports open up opportunities for developing robust and efficient artificial systems for sunlight to chemical energy conversion. Thermodynamic efficiency, in particular, requires that the redox potentials of light absorbing, charge transport, and catalytic components are closely matched. In this respect, the precision by which redox properties of atomically defined, molecular units can be selected and manipulated is particularly important. Artificial photosynthetic systems using organometallic components are attractive for the reason.[1] With the goal of combining the advantages of molecular components with the robustness of inorganic materials, we are exploring photocatalytic units consisting of an all-inorganic hetero-binuclear charge-transfer group that absorbs deep in the visible and is linked to a metal oxide-type multi-electron transfer catalyst. The binuclear group acts as light powered electron pump pulling electrons from (or donating to) the catalyst. By covalently anchoring the photocatalytic units on the surface of mesoporous silica materials such as MCM-41, the large surface area of the oxide support can be exploited to achieve a high density of reactive sites. Furthermore, the nanostructured features offer opportunities for ultimately arranging and coupling photocatalytic oxidation and reduction sites so that redox products are spatially separated.

One of the most challenging tasks of assembling an artificial photosynthetic system is the development of water oxidation sites that can be driven by visible light. The reason for focusing on oxygen evolving photocatalysts is that H_2O is the only viable

electron source for solar fuel generation.[2] We have recently demonstrated assembly and covalent anchoring of oxo-bridged hetero-binuclear groups like $TiOCr^{III}$,[3] $TiOCo^{II}$,[3,4] $TiOCu^{I}$,[5] $TiOSn^{II}$,[5] $ZrOCu^{I}$ [6] on the nanopore surface of MCM-41 silica material. The metal centers have oxygen as exclusive ligand. A $TiOCe^{III}$ group has been reported by Nakamura *et al.*[7] Mild synthetic methods leading to the selective formation of these heterobinuclear units at the expense of isolated centers have been developed.[3] The binuclear sites possess metal-to-metal charge-transfer (MMCT) absorptions across the visible region and feature donor metals with a considerable range redox potentials. In parallel work, we have demonstrated visible light-induced O_2 evolution from a water-oxidizing Ir oxide nanocluster coupled to a Cr^{VI} center inside MCM-41 silica pores.[8] Ir oxide nanoclusters are known from chemical and electrochemical oxidation studies to efficiently oxidize water to O_2.[9-12] Cr^{VI} has a visible light-absorbing ligand-to-metal charge-transfer chromophore (LMCT, Cr^{VI}-O^{II} $\rightarrow$ Cr^{V}-O^{I}) capable of driving the Ir oxide catalyst. The oxidized donor in this case is a transient hole on O, with a potential over +3 V. However, the minimal potential for O_2 evolution from H_2O is 1.23 V,[13] which implies that the Cr^{VI}-Ir oxide photocatalytic unit cannot be thermodynamically efficient. Therefore, a crucial step towards thermodynamically efficient photocatalytic water oxidation units is to replace the CrO LMCT chromophore by a binuclear MMCT pump because the redox potential of the donor center can be adjusted by selecting an appropriate metal with proper oxidation state. To this end, we have assembled a $TiOCr^{III}$ unit coupled to Ir oxide nanocluster in MCM-41 silica pores and report here the detection of water oxidation under visible light based on in situ FT-Raman and EPR spectroscopy.

2. Experimental

Binuclear TiOCr units were assembled in the mesopores of AlMCM-41 (Al/Si = 0.04) silica material by grafting $Ti^{III}(THF)_3Cl_3$ onto Cr-AlMCM-41. The synthetic method and chemicals used, along with a comprehensive spectroscopic characterization of TiCr-AlMCM-41 based on EXAFS, XANES, EPR, FT-Raman, FT-IR, optical spectroscopy and ICP analysis are described in a previous paper [3]. The Cr-AlMCM-41 starting material featuring single tetrahedral Cr^{VI} centers on the pore surface was prepared and characterized according to the method given in reference [8]. Ir oxide nanoclusters were prepared by adding of 3.5 g of this material to 50 mL toluene (distilled over CaH_2) containing 0.57 g $Ir(acac)_3$ (acac = acetyl acetonate) and stirring the solution for 4 h under N_2 atmosphere at RT. Subsequent calcination at 350^{o}C under O_2 flow resulted in the complete removal of the organic ligands and formation of Ir oxide nanoclusters as indicated by the intense, characteristic visible absorption band with an onset in the blue spectral region, Figure 1B spectrum (c) (Ir/Cr = 3.3 per ICP analysis). Confirmation of the formation of Ir_xO_y nanoclusters inside the silica mesopores was provided by high resolution transmission electron microscopy, as presented in a previous report.[8]

In order to probe for water oxidation under visible light excitation of the photocatalytic units using mass spectrometric detection, 150 mg of Ir oxide-TiCr-AlMCM-41 powder was suspended in 80 mL aqueous solution in a pyrex bulb (pH 5.4 – 5.7, buffer $NaHCO_3$ + Na_2SiF_6, or $Na_2B_4O_7$ + KH_2PO_4, solution made air-free by Ar bubbling and evacuation).[8] When probing for photocatalytic activity by in situ FT-

Raman or EPR spectroscopy, 15 mg of photocatalyst sample was loaded into a quartz tube and evacuated for 1 h before aqueous solution was added under N_2. For photolysis, the 458 nm emission of an Ar ion laser (Coherent model Innova 90-6) was used.

Optical spectra were measured on a Shimadzu model UV-2100 spectrometer equipped with an integrating sphere model ISR260. Mesoporous silica powder was pressed into a self-sustaining pellet and mounted in a home-built vacuum cell for diffuse reflectance measurements. Barium sulfate was used as reference. FT-Raman spectra were recorded with a Bruker model FRA-106 module of an IFS66V spectrometer equipped with a Nd:YAG laser source emitting at 1.064 μm (9394.3 cm^{-1}, 525 mW) and a liquid N_2 cooled Ge detector. Samples for FT-Raman measurement were prepared by loading the photocatalyst powder into a quartz tube. X-band electron paramagnetic resonance (EPR) spectra were recorded on a Varian E-109 spectrometer equipped with an E-102 microwave bridge (microwave frequency 9.25 GHz). The temperature of the sample was maintained at 20 K during the measurements using an Air Products Helitran liquid helium cryostat. Relative spin concentration was calculated by double integrating the first derivative EPR spectrum. For these calculations, and for simulation of EPR spectra, the Bruker WINEPR software was used.

3. Results and Discussion

In the TiCr-AlMCM-41 material, the majority of Cr centers are linked to a Ti center via an oxo bridge by virtue of selective redox coupling of the Ti^{III} precursor with Cr^{VI}.[3] Following calcination of the sieve at 350 ^{o}C, EPR spectroscopy revealed that the Cr centers exist as distorted octahedral Cr^{III} (shown in Figure 1A(a)) along with Cr^{V} in pyramidal or distorted tetrahedral coordination (Supporting Information).[14] The optical diffuse reflectance spectrum possesses a continuous Ti^{IV}-O-Cr^{III} → Ti^{III}-O-Cr^{IV} metal-to-metal charge-transfer (MMCT) absorption extending from about 350 nm to beyond 600 nm.[3] The MMCT band is shown as shaded area in Figure 1B between the absorption of TiCr^{III}-AlMCM-41 (trace b) and the sum of Cr^{III}-AlMCM-41 (trace a) + Ti-MCM-41. The EPR spectrum of the filtered, washed and dried product after reaction with the $Ir(acac)_3$ precursor showed a strong growth of Cr^{III} at the expense of Cr^{V} confirming that Ir^{III} precursor undergoes redox reaction with Cr centers. No Cr^{VI} was detected which, if present, would have a characteristic symmetric O=Cr^{VI}=O stretch absorption at 987 cm^{-1} (dehydrated) or 904 cm^{-1} (hydrated).[14] EPR spectrum Figure 1A(b) indicates that upon mild calcination to form Ir oxide nanocluster, most Cr centers remain in oxidation state III; at most 2 percent is converted to Cr^{V} based on spin counts. No Cr^{VI} is detected according to optical (Figure 1B(c)) and FT-IR spectroscopy.[14] We conclude that the resulting Ir_xO_y-TiCr-AlMCM-41 silica material has the majority of the Cr centers in the form of Cr^{III} linked to a Ti centers.[15] Overlap of the visible absorption of Ir oxide nanoclusters with the MMCT band is minimal around 460 nm. Hence, photolysis experiments were conducted with laser emission at this wavelength.

An aqueous suspension of Ir oxide nanocuster-containing $TiCr^{III}$-AlMCM-41 particles with added persulfate ($Na_2S_2O_8$, $1.1x10^{-2}$M), an established acceptor for water oxidation half reactions [10-12], was irradiated with the 458 nm beam of an Ar ion laser (beam diameter 1 in., 170 mW). Periodic mass spectrometric sampling of the content of the gas phase above the solution according to procedures described previously [8] did not show evolution of O_2 in the gas phase. On the other hand, monitoring of the aqueous suspension by FT-Raman spectroscopy revealed formation of superoxide species. As can be seen in Figure 2 from the comparison of spectra before (a) and after (b) 30 min. illumination with 458 nm light, a band appears at 994 cm^{-1} as a consequence of the photolysis. The bands at 1077 and 980 cm^{-1} are due to persulfate acceptor and its product SO_4^{2-}, respectively.[16] When conducting the photolysis with $H_2{}^{18}O$, product bands appear at 961 and 930 cm^{-1} (Figure 2(c)). The observed isotope shifts are in agreement with those reported for $^{16}O^{18}O$ and $^{18}O^{18}O$ bond modes, and the frequency falls into the typical range for superoxide species.[17] Observation of ^{18}O labeled product directly proves that water molecules are oxidized. The appearance of isotopically mixed superoxide in addition to fully labeled product, but no parent isotope when using ^{18}O labeled water indicates isotope exchange during reaction, most likely with the Ir oxide catalyst. Understanding of the observed isotope distribution requires elucidation of the detailed water oxidation mechanism on the Ir oxide nanocluster surface, currently underway in our laboratory.

Formation of superoxide species was confirmed by EPR spectroscopy. After 30 min. of 458 nm irradiation, an EPR signal with $g_1 = 2.034$, $g_2 = 2.010$, $g_3 = 2.005$ was observed, as shown in Figure 3(b). The g values are characteristic of superoxide species bound to a tetrahedral Ti^{IV} center, $O_2^{-\cdots}Ti$.[18,19] The simulated EPR spectrum, Figure 3(c), is in good agreement with the experimental observation and further confirms the superoxide assignment of the EPR signal. The simulated O_2^- (S=1/2) signal is described by parameters: g(x) = 2.005, g(y) = 2.010, g(z) = 2.034; linewidth x- direction =12 G, y-direction = 12 G, and z-direction = 20 G. This spectrum was not observed prior to photolysis (trace (a)). The 458 nm irradiation did not result in any change of the intensity of the Cr^{III} EPR signal (β signal of distorted octahedral Cr^{III} with $g_{iso} = 2.014$; uncertainties of g values are $\pm$ 0.002).[15] Similarly, the Cr^V absorption exhibits little change upon photolysis.

The formation of superoxide is explained by the photocatalytic oxidation of water at Ir oxide nanoclusters. This oxide, whether in the form of a colloid [12] or nanoclusters occluded in silica pores [8] is known to evolve O_2. Turnover frequencies similar to the ones observed for the natural water oxidation complex have been reported.[12] In the presence of transient Ti^{III}, trapping of dissolved O_2 by the metal centers will occur.[18,19] Hence, upon excitation of the Ti^{IV}-O-Cr^{III} $\rightarrow$ Ti^{III}-O-Cr^{IV} charge-transfer units, the oxidizing Cr^{IV} donor centers (E^o = +2 V in acid solution, but likely lower in the solid oxide coordination environment)[13] pull electrons, one at the time, from Ir oxide nanocluster while being reduced back to the Cr^{III}. At the same time, transient Ti^{III} is reoxidized by persulfate to Ti^{IV}, thereby restoring the visible MMCT chromophore. As

photooxidation of the Ir oxide catalyst proceeds, O_2 accumulating in solution begins to compete with persulfate for reaction with transient Ti^{III}, leading to the formation of the observed $O_2^{-\cdots}Ti$ species.[18,19]

The proposed mechanism for superoxide formation is supported by the observation that Ti^{III} ($g_\perp = 1.986$, $g_\parallel = 1.965$),[20] rather than superoxide, is formed if the persulfate acceptor is absent in the photolysis experiment, as shown in Figure 4A, trace (a) (as expected, no superoxide band appears in the Raman spectrum, Figure 2(d)). A simulated superposition, shown in Figure 4A trace (b), of the Ti^{III} signal and a small signal originating from Cr^V agrees well with the experimental spectrum. The corresponding simulated components are shown in Figure 4B: Trace (a) gives the Ti^{III} (S=1/2) component using g(x) = g(y) = 1.986, g(z) = 1.965; linewidth: x-direction = y-direction = 10 G, z-direction = 30 G; trace (b) shows the simulated Cr^V(S=1/2) signal (g(x) = 1.977, g(y) = 1.970, g(z) = 1.955; linewidth: x-direction = 18 G, y-direction = 8 G, z-direction = 22 G). The latter reproduces well a small Cr^V signal observed when conducting the photolysis experiment, again in the absence of persulfate acceptor, with (Ti-free) samples of Ir_xO_y-Cr-AlMCM-41, presented in Figure 4A(c). Inclusion of the Cr^V signal (which is due to Cr sites with a rhombic coordination sphere) [21] as a component in the simulated spectrum, Figure 4A(b), gives a good match with the observed signal Figure 4A(a). Note that the shallow slope of the observed signal on the low field side, not reproduced by the simulation, is due to the much broader Cr^{III} signal. No change of the Cr^{III} EPR signal intensity is noted upon visible light irradiation of the MMCT chromophore, indicating that transient Cr^{IV} is spontaneously re-reduced by the Ir

oxide nanocluster. We conclude that visible light irradiation of Ir_xO_y-TiCr-AlMCM-41 in water in the absence of persulfate results in the buildup of Ti^{III}, which is explained by the fact that no acceptor is present that would re-oxidize the photo-reduced Ti. As the MMCT absorption is depleted upon irradiation, photooxidation of the Ir oxide clusters ceases and no O_2 is formed. The steady state buildup of Ti^{III} implies that Ir oxide nanoclusters are efficiently coupled to the Cr centers. Specifically, we conclude from these observations that electron donation from Ir oxide cluster to transient Cr^{IV} competes successfully with back electron transfer from Ti^{III}, which is consistent with the established efficient hole acceptor properties of Ir oxide.

4. Conclusions

We have demonstrated a functional water oxidation catalyst driven by a hetero-binuclear visible light charge-transfer pump on a nanoporous solid support. The flexibility of assembling such all-inorganic molecular charge-transfer sites and coupling to a multi-electron transfer catalyst opens up the development of robust photocatalysts in nanoporous scaffolds with tailored light absorption properties and matched redox potentials. With the concept demonstrated, future effort will focus on the determination of the detailed kinetics of photo-induced electron transfer within the unit. These measurements will serve as a vehicle for determining quantum efficiencies and improving them by synthetically manipulating the coupling between charge-transfer chromophore and catalyst.

Acknowledgment

This work was supported by the Director, Office of Science, Office of Basic Energy Sciences, Division of Chemical, Geological and Biosciences of the U.S. Department of Energy under Contract No. DE-AC03-76SF00098. The authors thank Drs. Vittal Yachandra and Yulia Pushkar for access to their EPR laboratory and help with the experiments.

References

[1] Sun, L; Hammarstrom, L.; Akermark, B.; Styring, S. *Chem. Soc. Rev.* **2001**, *30*, 36-49.

[2] Lewis, N. S.; Nocera, D. G. *Proc. Natl. Acad. Sci. USA* **2006**, *103*, 15729-15735.

[3] Han, H.; Frei, H. *J. Phys. Chem. C* **2008**, *112*, 000 (Web Release May 3, 2008; DOI 10.1021/jp800556g).

[4] Han, H.; Frei, H. *Microporous Mesoporous Mater.* **2007**, *103*, 265-272.

[5] Lin, W.; Frei, H. *J. Phys. Chem. B* **2005**, *109*, 4929-4935.

[6] Lin, W.; Frei, H. *J. Am. Chem. Soc.* **2005**, *127*, 1610-1611.

[7] Nakamura, R.; Okamoto, A.; Osawa, H.; Irie, H.; Hashimoto, K. *J. Am. Chem. Soc.* **2007**, *129*, 9596.

[8] Nakamura, R.; Frei, H. *J. Am. Chem. Soc.* **2006**, *128*, 10668-10669.

[9] Lehn, J. M.; Sauvage, J. P.: Ziessel, R. *Nouv. J. Chim.* **1980**, *4*, 355-358.

[10] Harriman, A.; Pickering, I. J.; Thomas, J. M.; Christensen, P. A. *J. Chem. Soc., Faraday Trans. 1* **1988**, *84*, 2795-2806.

[11] Mills, A.; Russell, T. *J. Chem. Soc., Faraday Trans.* **1991**, *87*, 1245-1250.

[12] Morris, N. D.; Suzuki, M.; Mallouk, T. E. *J. Phys. Chem. A* **2004**, *108*, 9115-9119.

[13] *Standard Potentials in Aqueous Solution;* (Eds. Bard, A. J.; Parson, R.; Jordan, J.) Marcel Dekker: New York, 1985.

[14] Supporting Information

[15] Comprehensive spectroscopic characterization of TiCr-AlMCM-41 based on EXAFS, XANES, EPR, FT-Raman, FT-IR and optical spectroscopy is presented in Ref. 3.

[16] Yang, C.Q.; Gu, X. *J. Appl. Polym. Sci.* **2001**, *81*, 223-228.

[17] Nakamoto, K. *Infrared and Raman Spectra of Inorganic and Coordination Compounds, Part B, 5th ed.;* Wiley: New York, 1997; p. 154-168.

[18] Lunsford, J. H. *Catal. Rev.* **1973**, *8*, 135-157.

[19] Bal, R.; Chaudhari, K.; Srinivas, D.; Sivasankar, S.; Ratnasamy, P. *J. Mol. Catal. A.: Chemical* **2000**, *162*, 199-207.

[20] Howe, R. F.; Gratzel, M. *J. Phys. Chem.* **1985**, *89*, 4495-4499.

[21] Weckhuysen, B.M.; Schoonheydt, R.A.; Mabbs, F.E.; Collison, D. *J. Chem. Soc. Faraday Trans.* **1996**, *93*, 2431-2436.

Figure Captions

Fig. 1: TiCr-AlMCM-41 and Ir_xO_y-TiCr-AlMCM-41. (A) X-band EPR spectra of Cr^{III} of (a) TiCr-AlMCM-41 calcined at 350 ^oC. (b) Ir_xO_y-TiCr-AlMCM-41 calcined at 350 ^oC. β signal, g_{iso} = 2.029, width 600 G. Spectra were recorded at 20 K. (B) Diffuse reflectance spectra of (a) Cr^{III}-AlMCM-41; (b) $TiCr^{III}$-AlMCM-41. The shaded area is due to the Ti^{IV}-O-Cr^{III} → Ti^{III}-O-Cr^{IV} MMCT absorption;[3] (c) Ir_xO_y-$TiCr^{III}$-AlMCM-41 after calcination at 350 ^oC.

Fig. 2: FT-Raman spectra of Ir_xO_y-TiCr-AlMCM41 (a) before photolysis with 458 nm Ar-ion laser in the presence of sodium persulfate in $H_2{}^{16}O$; (b) after photolysis for 30 min in the presence of sodium persulfate in $H_2{}^{16}O$; (c) after photolysis for 30 min in the presence of sodium persulfate in $H_2{}^{18}O$; and (d) after photolysis for 30 min in the presence of in $H_2{}^{16}O$ without sodium persulfate.

Fig. 3: EPR spectra of 458 nm photolysis (170 mW) of Ir_xO_y-TiCr-AlMCM-41 in aqueous solution containing $Na_2S_2O_8$ acceptor. (a) before, (b) after 30 min photolysis, and (c) simulated EPR spectrum of superoxide (O_2^-). Superoxide signal was not observed when conducting the photolysis experiment with Ir_xO_y-Ti-MCM-41 sample. Slanting of the curves to the right is due to the signal of residual Cr^V. Spectra were recorded at 20 K.

Fig. 4: Panel A: EPR spectra of (a) aqueous Ir_xO_y-TiCr-AlMCM-41 suspension in the absence of sodium persulfate after 30 min photolysis with 458 nm Ar-ion laser emission at 110 mW. (b) Superposition of simulated Ti^{III} and Cr^{V} spectra. (c) aqueous suspension of Ir_xO_y-Cr-AlMCM-41 (no Ti) in the absence of persulfate after 30 min photolysis with 458 nm light. Panel B: Simulated EPR spectra of (a) Ti^{III}, (b) of Cr^{V}.

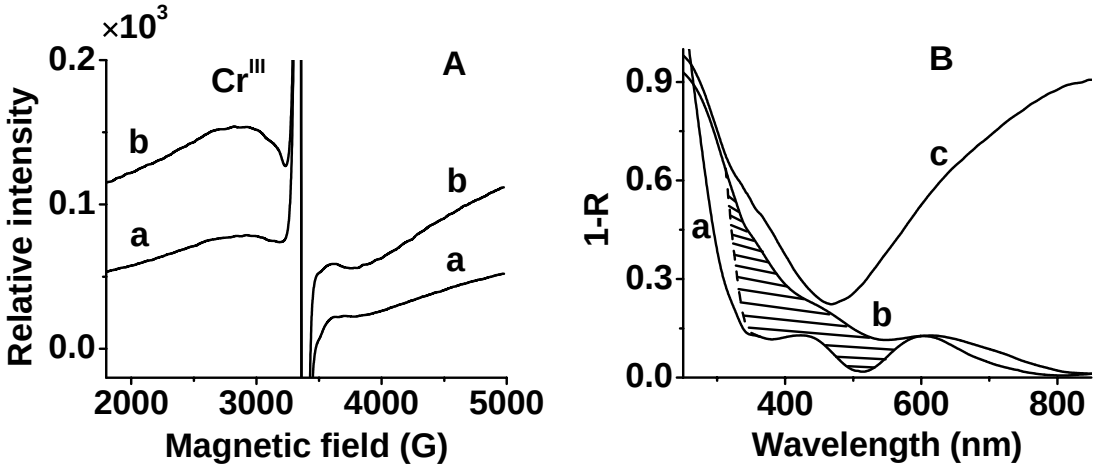

Fig. 1: TiCr-AlMCM-41 and Ir_xO_y-TiCr-AlMCM-41. (A) X-band EPR spectra of Cr^{III} of (a) TiCr-AlMCM-41 calcined at 350 ^oC. (b) Ir_xO_y-TiCr-AlMCM-41 calcined at 350 ^oC. β signal, g_{iso} = 2.029, width 600 G. Spectra were recorded at 20 K. (B) Diffuse reflectance spectra of (a) Cr^{III}-AlMCM-41; (b) $TiCr^{III}$-AlMCM-41. The shaded area is due to the Ti^{IV}-O-Cr^{III} → Ti^{III}-O-Cr^{IV} MMCT absorption;[3] (c) Ir_xO_y-$TiCr^{III}$-AlMCM-41 after calcination at 350 ^oC.

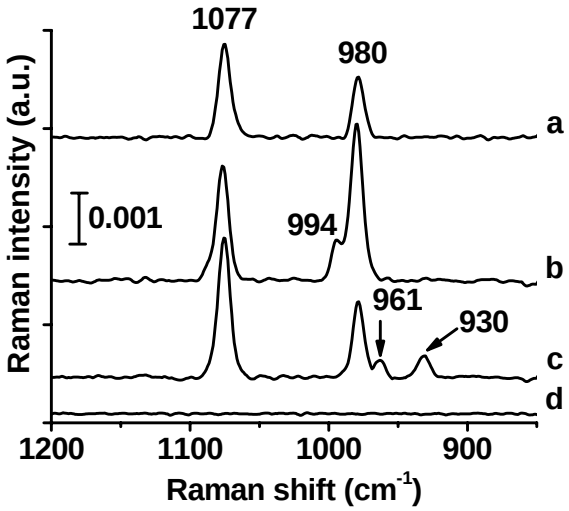

Fig. 2: FT-Raman spectra of Ir_xO_y-TiCr-AlMCM41 (a) before photolysis with 458 nm Ar-ion laser in the presence of sodium persulfate in $H_2{}^{16}O$; (b) after photolysis for 30 min in the presence of sodium persulfate in $H_2{}^{16}O$; (c) after photolysis for 30 min in the presence of sodium persulfate in $H_2{}^{18}O$; and (d) after photolysis for 30 min in the presence of in $H_2{}^{16}O$ without sodium persulfate.

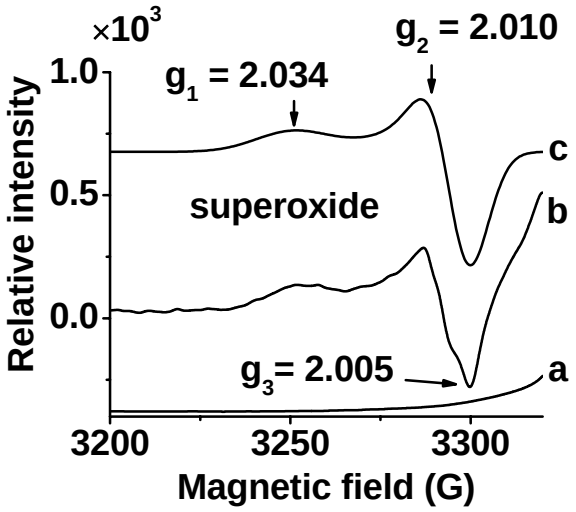

Fig. 3: EPR spectra of 458 nm photolysis (170 mW) of Ir_xO_y-TiCr-AlMCM-41 in aqueous solution containing $Na_2S_2O_8$ acceptor. (a) before, (b) after 30 min photolysis, and (c) simulated EPR spectrum of superoxide (O_2^-, S=1/2) with the following parameters: g(x) = 2.005, g(y) = 2.010, g(z) = 2.034; linewidth x-direction =12 G, y-direction = 12 G, and z-direction = 20 G. Superoxide signal was not observed when conducting the photolysis experiment with Ir_xO_y-Ti-MCM-41 sample. Slanting of the curves to the right is due to the signal of residual Cr^V. Spectra were recorded at 20 K.

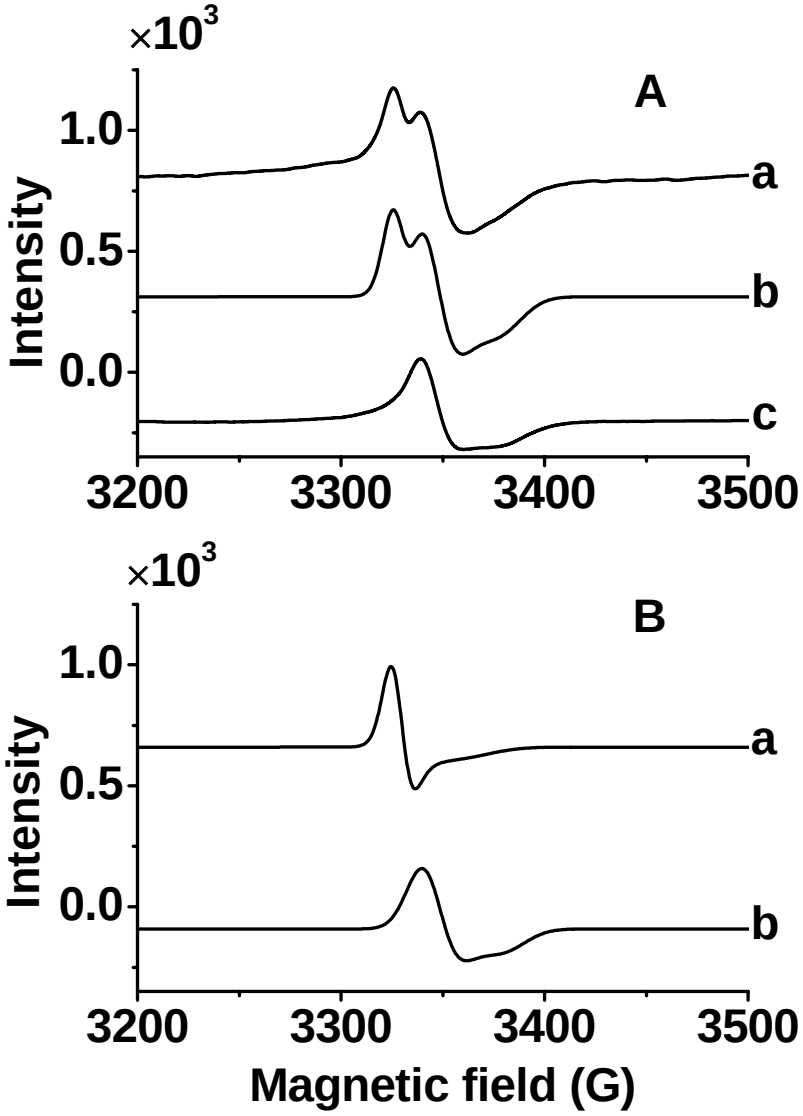

Fig. 4: Panel A: EPR spectra of (a) aqueous Ir_xO_y-TiCr-AlMCM-41 suspension in the absence of sodium persulfate after 30 min photolysis with 458 nm Ar-ion laser emission at 110 mW. (b) Superposition of simulated Ti^{III} and Cr^{V} spectra. (c) aqueous suspension of Ir_xO_y-Cr-AlMCM-41 (no Ti) in the absence of persulfate after 30 min photolysis with 458 nm light. Panel B: Simulated EPR spectra of (a) Ti^{III}, (b) of Cr^{V}.